Nano Energy 36 (2017) 295–302

Contents lists available at ScienceDirect

Nano Energy

journal homepage: www.elsevier.com/locate/nanoen

Full paper

Cost-effective sustainable-engineering of $CH_3NH_3PbI_3$ perovskite solar cells through slicing and restacking of 2D layers

Congcong Wu[a,*,1], Haijin Li[a,b,1], Yongke Yan[a], Bo Chi[b,*], Jian Pu[b], Jian Li[b], Mohan Sanghadasa[c], Shashank Priya[a,*]

[a] Center for Energy Harvesting Materials and System (CEHMS), Virginia Tech, Blacksburg, VA 24061, USA
[b] Center for Fuel Cell Innovation, School of Materials Science and Engineering, Huazhong University of Science & Technology, Wuhan 430074, China
[c] Aviation and Missile Research, Development, and Engineering Center, US Army RDECOM, Redstone Arsenal, AL, USA

ARTICLE INFO

Keywords:
Perovskite
2D layers
Slice
Restack
Sustainable solvent

ABSTRACT

Owing to their high conversion efficiency and potentially cost-effective manufacturing, organic–inorganic lead halide perovskite solar cells (PSCs) have been dominant photovoltaic research topic in this decade. The photovoltaic performance of PSCs is highly dependent upon the quality of perovskite layer. In order to advance the deployment of PSCs, fabrication of high-quality perovskite film using a facile and sustainable process is essential. This study provides significant breakthrough in this direction. A novel fabrication process is demonstrated that allows slicing of 2D layers from single crystals and restacking them to fabricate high-quality perovskite film. The discovery that CH_3NH_2 can slice the 3D $CH_3NH_3PbI_3$ perovskite crystal into 2D layered perovskite intermediates via intercalation process opens a new pathway for pursuing synthesis of a variety of photovoltaic materials. The 2D layered intermediate shows high solubility in acetonitrile (ACN) solvent, which is considered as a replacement for N, N-dimethylformamide (DMF) in order to enable sustainable processing. This solvent system enables fabrication of high-quality perovskite layer by one-step synthesis method. Based on this cost-effective sustainable synthesis approach, low temperature processed PSC was found to match the performance of PSC synthesized using high temperature process.

1. Introduction

Three-dimensional (3D) organic-inorganic perovskite solar cells (PSCs) have attracted tremendous academic and industrial interests as potential candidate for next generation low-cost high-efficiency photovoltaic device [1,2]. The highest reported efficiency of PSCs has exceeded 22% [3], which is comparable to the state-of-the-art crystalline silicon solar cell. At this juncture, there are two major challenges in advancing the deployment of PSCs, namely, cost-effective sustainable manufacturing and environmental stability. Generally, the fabrication of perovskite film begins with the reaction of perovskite precursors followed by solution deposition (one-step synthesis and two-step synthesis) or vapor deposition process. For solution deposition, in order to achieve high-quality perovskite film, various processing methods including anti-solvent [4,5], surface induction [6,7], stoichiometry tailoring [8,9], and solvent annealing [10–12] etc. have been employed to modulate the crystallization kinetics of perovskites. However, these delicate processes show limited reproducibility and require complex procedure, which necessitates the tight process control to facilitate perovskite formation. In contrast, homogeneous perovskite films can be readily fabricated by using vapor deposition, but the vacuum based technique is expensive [13], which reduces the cost-effectiveness of PSCs. Particularly, the limitation of the complex and expensive processes become more prominent in scaling up the fabrication of PSCs. The industrial production of PSCs requires printable processes (slot die, roll-to-roll), however, realizing this process not only faces material level challenges that require high availability of environment-friendly materials, but also challenges in terms of the facile fabrication process that is compatible with the scaling. In order to advance the commercialization of PSCs, development of a facile, reproducible, industrially-compatible sustainable fabrication process is critical.

To resolve this processing challenge, we developed an entirely new method for perovskite film fabrication, which allows extraction of 2D layers from 3D single crystals. Perovskite single crystals (AMX_3) have low trap-state density and high carrier lifetime [14]. A desired

* Corresponding authors.
E-mail addresses: ccw39@vt.edu (C. Wu), chibo@hust.edu.cn (B. Chi), spriya@vt.edu (S. Priya).
[1] These authors contributed equally to this work.

http://dx.doi.org/10.1016/j.nanoen.2017.04.034
Received 8 March 2017; Received in revised form 12 April 2017; Accepted 13 April 2017
Available online 21 April 2017

approach for synthesis of perovskite film will be to slice the 3D perovskite crystals into 2D layers and restack them to form thin film structure. This approach removes the step required for transition of perovskite precursors into crystallized perovskites and enables crystal based thin film fabrication. Traditionally, two-dimensional (2D) layered counterparts from 3D perovskites have been realized by partial or full substitution of A-site ion with a larger size cation [15–17]. The interaction between the substituted cation and 3D frameworks plays a crucial role in determining the structural dimensionality.

Zhou et al. have reported the CH_3NH_2 gas induced method for synthesizing a highly crystallized uniform perovskite film [18]. When exposed to the CH_3NH_2 gas, $CH_3NH_3PbI_3$ reacts with CH_3NH_2 and rapidly forms a liquid intermediate phase. On degassing the CH_3NH_2 gas, the intermediate phase turns back to perovskite. By using this approach, synthesis of highly oriented and crystallized perovskite film can be achieved. It has been hypothesized that the liquid intermediate results from the collapse of PbI_6-octahedra framework. Building upon this hypothesis, we sought to discover the specific mechanism behind the interaction between CH_3NH_2 and the $CH_3NH_3PbI_3$ perovskite, and use this interaction to manipulate the transformation of 3D crystals into perovskite thin film.

The results of this study demonstrate success in slicing of 3D perovskite crystals into 2D layers and restacking them for facile fabrication of $CH_3NH_3PbI_3$ perovskite thin film. Upon interaction with CH_3NH_2, the $CH_3NH_3PbI_3$ perovskite first turns into liquid intermediate phase and then gradually becomes a bleached solid phase. The solid phase is irreversible at room temperature and shows high orientation and excellent crystallinity. We propose an in-situ intercalation mechanism that could reveal the origin of this interaction. Upon CH_3NH_2 treatment of $CH_3NH_3PbI_3$ perovskite, CH_3NH_2 intercalates in the $CH_3NH_3PbI_3$ framework and slices the 3D perovskite into 2D layered structure. The 2D layered perovskite shows high solubility in acetonitrile (ACN) solvent. Utilizing the perovskite ACN solution, homogeneous and pinhole free $CH_3NH_3PbI_3$ perovskite films were fabricated through one-step spin coating. Upon evaporation of ACN and excess CH_3NH_2, the 2D layered perovskite intermediates were restacked forming high-quality perovskite film. The employment of ACN avoids the use of potentially toxic N, N-dimethylformamide (DMF) as solvent. In addition, ACN provides safer reaction medium, better life cycle and lower waste-handling issues, which leads to sustainable PSC fabrication [19,20]. By employing the sustainable solvent system, we fabricated low-temperature processed cell with a conversion efficiency of 15.9%, which was similar to that of PSC fabricated using high temperature annealing process.

2. Experimental section

2.1. Materials

CH_3NH_3I (MAI) and 2,2,7,7-tetrakis(N,N-di-4-methoxyphenylamino)-9,9-spirobifluorene(Spiro-OMeTAD) were obtained from Luminescence Technology Corp. Methylamine solution (33 wt% in absolute ethanol), PbI_2, acetonitrile (ACN), γ-Butyrolactone, Dimethylsulfoxide (DMSO), N,N-dimethylformamide (DMF), toluene, chlorobenzene, diethyl ether, titanium isopropoxide (TTIP), α-terpineol, ethanol were purchased from Sigma-Aldrich. TiO_2 paste (18NR-T) was acquired from Dyesol. Fluorine-doped tin oxide (FTO) glass was purchased from Nippon Sheet Glass, and conductive flexible polymer substrate (ITO/PEN) was obtained from Peccell Technologies, Inc.

2.2. Synthesis of layered $CH_3NH_3PbI_3$ intermediate

The starting $CH_3NH_3PbI_3$ perovskite film was prepared on FTO glass by one-step synthesis using toluene as the anti-solvent and then annealed at 100 °C for 10 min. For short time CH_3NH_2 exposure treatment, we placed the $CH_3NH_3PbI_3$ film directly above the container with methylamine solution for 2 s and then removed it. For longtime exposure, we placed the $CH_3NH_3PbI_3$ film in methylamine gas for 10 min~30 min until the irreversibly bleached film was formed. To prepare the $MAPbI_3$ crystals, 1.2 M solution of $CH_3NH_3PbI_3$ was

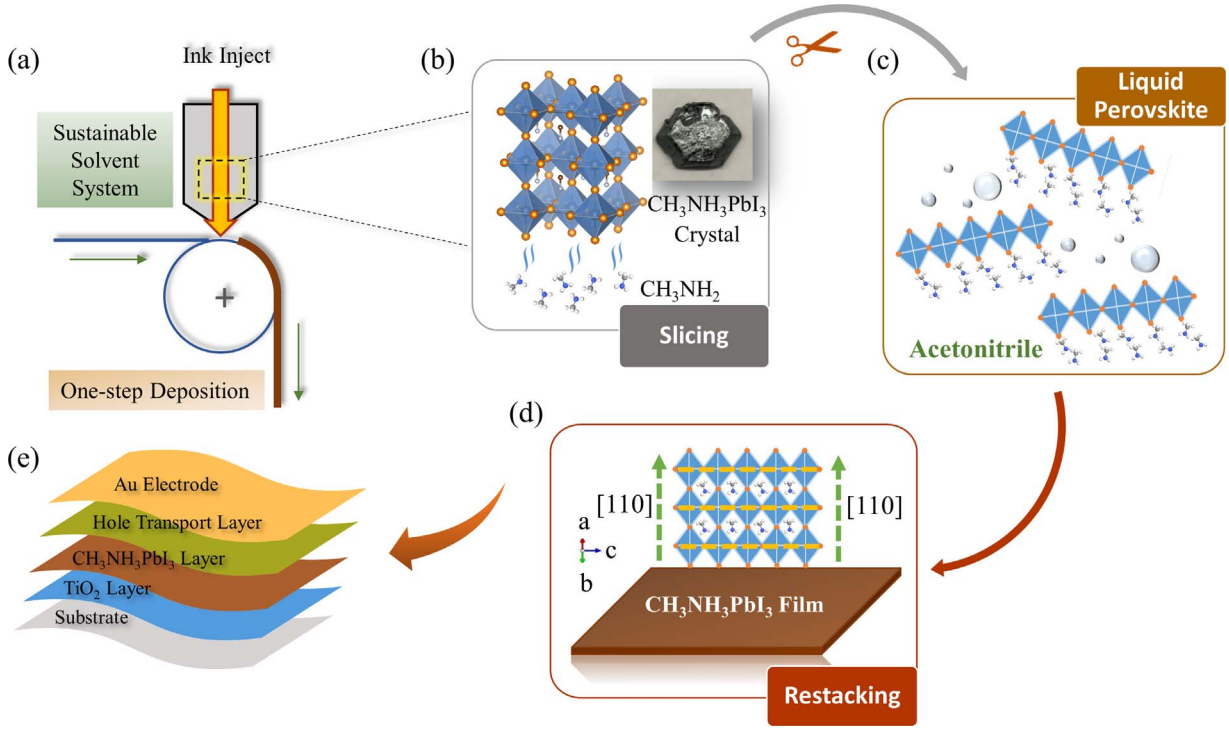

Fig. 1. (a) Schematics of printable roll-to-roll fabrication process. (b) The 3D crystal structure of $CH_3NH_3PbI_3$ perovskite and picture of $CH_3NH_3PbI_3$ single crystal. (c) With CH_3NH_2 gas exposure, the 3D perovskite was sliced into 2D colloidal sheets and the resultant 2D perovskite intermediate was dissolved in the solvent of acetonitrile. (d) Using the perovskite acetonitrile solution, the $CH_3NH_3PbI_3$ perovskite thin film was fabricated by one-step deposition method. The crystallized perovskite film was formed through restacking the 2D layered perovskite intermediates along [110] direction. (e) Structure of flexible PSCs prepared through slicing and restacking synthesis.

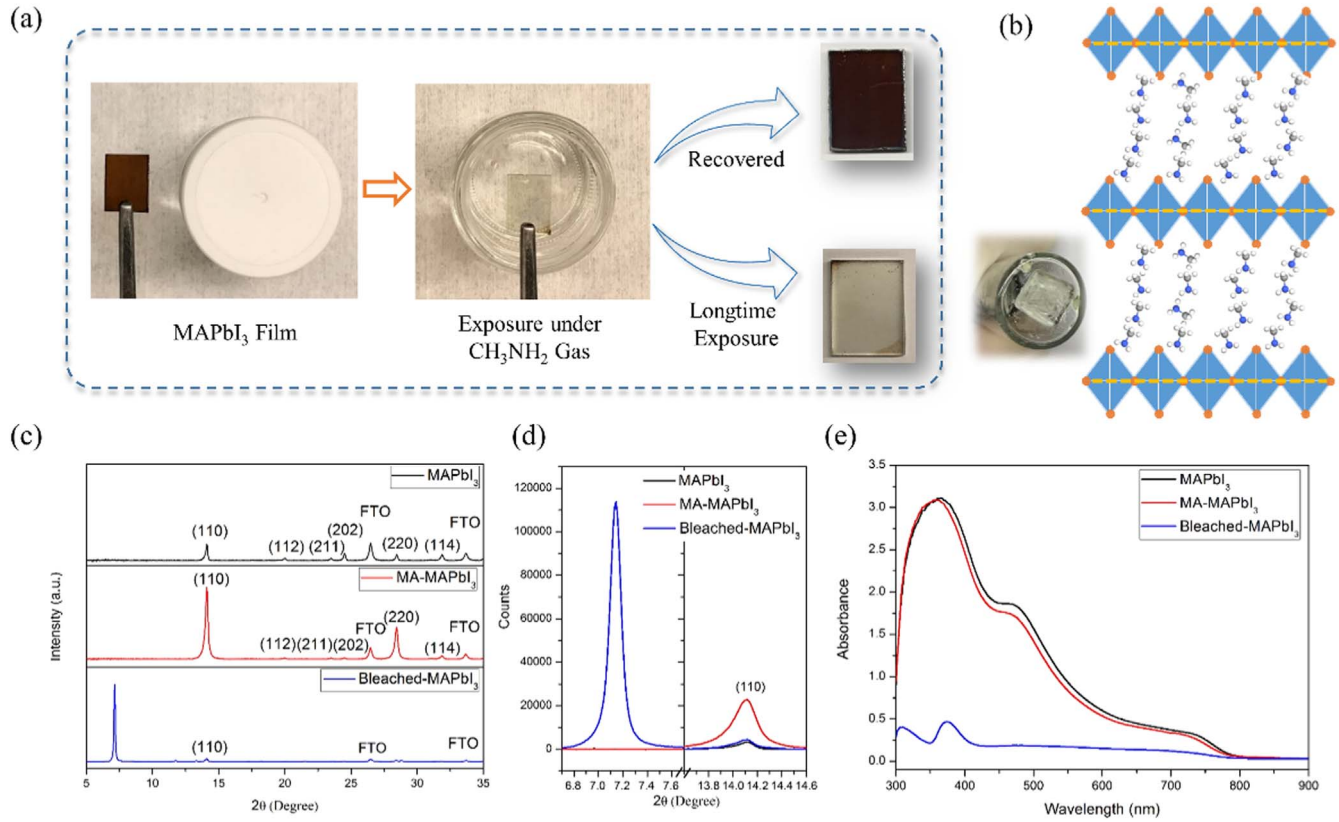

Fig. 2. (a) Demonstration of $CH_3NH_3PbI_3$ perovskite film evolution under the CH_3NH_2 gas exposure for different duration. (b) Schematics of 2D layered perovskite intermediates obtained through the interaction between CH_3NH_2 and $CH_3NH_3PbI_3$ perovskites. (c) XRD patterns of pristine $MAPbI_3$ perovskite film, MA-$MAPbI_3$ film, and bleached $MAPbI_3$ film. (d) Comparison of XRD peak intensity at 2θ=7.1° and 14.1°, respectively. (e) UV–vis absorption spectra of pristine $MAPbI_3$ perovskite film, MA-$MAPbI_3$ film, and bleached $MAPbI_3$ film.

prepared by dissolving PbI_2 and MAI (molar ratio 1:1) in γ-butyrolactone and filtered in the vial. After that, the vial was inserted in an oil bath and slowly heated to 110 °C and kept for 4 h. Once $CH_3NH_3PbI_3$ crystals were formed at the bottom of vial, they were washed with diethyl ether and dried under nitrogen gas. A calculated amount of $CH_3NH_3PbI_3$ crystals were placed in a vial that was then packed in a sealed bottle with methylamine solution and held overnight. The evaporated methylamine gas diffused into the vial and reacted with $CH_3NH_3PbI_3$ crystals, forming the layered perovskite intermediate.

2.3. Device fabrication

For the preparation of high temperature TiO_2 based mesoporous PSCs, TiO_2 compact layer was first fabricated through spin-coating mildly acidic TTIP solution at 2000 rpm for 20 s on FTO glass. TiO_2 mesoporous paste was prepared by diluting 18NR-T paste with α-terpineol and ethanol and spin-coating on top of TiO_2 compact layer, followed by annealing at 500 °C for 1 h. The low-temperature PSC and flexible PSC were prepared by depositing the low-temperature TiO_2 paste on FTO glass and flexible polymer substrate, respectively. The detailed fabrication process of low-temperature TiO_2 is described elsewhere [21]. The $CH_3NH_3PbI_3$ perovskite layer was prepared from liquid perovskite ACN solution. The $CH_3NH_3PbI_3$ layered intermediates were dissolved in ACN to form a solution with different concentration. After that, the solution was spin-coated on the substrate at 4000 rpm for 20 s with and without further treatment. The annealing process was conducted on a hotplate at 100 °C for 10 min, and the vacuum process was performed in a vacuum chamber at ~10^{-3} Torr. Next, the Spiro-OMeTAD solution was spin-coated on perovskite layer at 4000 rpm for 20 s. Lastly, 80 nm of gold was thermally evaporated as metal electrode over the active area of each device fixed at 0.096 cm^2.

2.4. Characterizations

X-ray diffraction (XRD) patterns were measured using Philips Xpert Pro X-ray diffractometer (Almelo, The Netherlands). UV–vis absorption spectra were recorded using UV–vis spectrophotometer (U-4100, Hitachi). The morphology of film was examined by scanning electron microscopy (SEM, Quanta 600 FEG, FEI). A solar simulator (150 W Sol 2ATM, Oriel) was employed to provide air mass (AM 1.5) illumination of 100 mW cm^{-2}. A Keithley digital source meter (Model 2400) was employed to measure the J-V characteristics of the solar cells.

3. Results and discussion

Fig. 1 illustrates the whole procedure that is compatible with large-scale, printable fabrication process for PSCs. This process uses sustainable solvent alternative and enables simple one-step deposition for perovskite film fabrication. Implementation of the process allows slicing $CH_3NH_3PbI_3$ crystals into 2D layered perovskite intermediates and then utilizing the perovskite ACN solution to fabricate $CH_3NH_3PbI_3$ thin film. The fabrication begins with $CH_3NH_3PbI_3$ single crystal, consisting of a 3D framework of corner-sharing MX_6 octahedra, where A is located in the 12-fold coordinated hole in the octahedra, as shown in Fig. 1b. The size of A-site cation should be according to the size of hole to maintain the 3D perovskite structure [22,23]. In 3D $CH_3NH_3PbI_3$ perovskites, $CH_3NH_3^+$ fills in the A-site via hydrogen bonding with halogens. If $CH_3NH_3^+$ is replaced or mixed with larger size cation, due to the confinement of the octahedra, the 3D structure tends to transform to a layered 2D structure, where MX_6 corner-sharing octahedra layers are spaced between intercalated cations [24–26]. In this study, CH_3NH_2 was employed as a medium to enable the transformation from 3D crystal to 2D layered sheets. Upon exposure to

CH_3NH_2 gas, the ammonium in CH_3NH_2 can form the hydrogen bond with halogens in MX_6 octahedra (N-H···I).

In tetragonal $CH_3NH_3PbI_3$ perovskite, (110) is the close-packed plane with highest atomic density. The dislocation occurs most easily along [110] direction [27,28]. Owing to the lowest energy required for the planar dislocation, CH_3NH_2 acts as a "scissor", slicing the 3D perovskite crystal along the (110) plane. Upon exposure to CH_3NH_2 gas, the solid 3D structure exfoliates into colloidal sheets along (110) plane. The resultant 2D perovskite intermediate shows high solubility in ACN solvent, and by using this perovskite ACN solution, the $CH_3NH_3PbI_3$ perovskite film can be readily fabricated through simple one-step deposition method, as shown in Fig. 1c. With the evaporation of ACN and release of CH_3NH_2, the layered perovskite intermediates restack along [110] direction, forming a high-quality excellent-crystallinity $CH_3NH_3PbI_3$ thin film (Fig. 1d).

To gain further insight and reinforce our proposition on the interaction between CH_3NH_2 and $CH_3NH_3PbI_3$ perovskite, we systematically investigated the reaction of CH_3NH_2 with $CH_3NH_3PbI_3$ thin film. Fig. 2a depicts the evolution of $CH_3NH_3PbI_3$ perovskite film under the CH_3NH_2 gas exposure. The perovskite film bleached rapidly upon CH_3NH_2 gas exposure, and turned back to dark perovskite immediately when removed from the CH_3NH_2 gas. This transformation behavior is shown in Movie S1. This transformation from perovskite to bleached intermediate state is reversible. With transient exposure, owing to the weak van der Waals type interaction between the sliced MX_6 layers, the CH_3NH_2 can readily deintercalate when removed from the exposure to CH_3NH_2 gas, leading to recovery of perovskite from exfoliated colloids [29]. However, if we extend the exposure time (10–30 min), the perovskite irreversibly turns into a bleached state at room temperature (Fig. 2a). With increasing exposure time, the intercalated CH_3NH_2 bonds to the MX_6 layers at both ends (^+H_3N-R-NH_3^+), removing the van der Waals gap. The confinement of the induced CH_3NH_2 leads to the transformation from 3D to 2D layered structure intermediate, where the MX_6 layers are spaced by the induced CH_3NH_2 species [15], as illustrated in Fig. 2b. The photo inserted in Fig. 2b shows the 2D layered crystals obtained through the interaction between CH_3NH_2 gas and $CH_3NH_3PbI_3$ single crystal. The hexagonal shape $CH_3NH_3PbI_3$ crystal converts to a well-defined square shape sheet. The intercalation of CH_3NH_2 in 3D perovskite causes the slicing of MX_6 octahedral sheet, leading to the formation of 2D layered crystal. The 2D layered perovskites have shown promising stability against moisture [25]. Fig. S1 shows the comparison of water-resistance between 3D $CH_3NH_3PbI_3$ perovskite film and 2D bleached film. The color of 3D perovskite film changed to yellow within 1s upon contact with water droplet, indicating the formation of PbI_2 due to perovskite decomposition. In contrast, the 2D bleached film remained unchanged upon contacting water droplet even up to 10 min. The high water-resistant bleached film further confirms the formation of 2D layered perovskites with intercalation of CH_3NH_2 into 3D perovskite crystal.

Fig. 2c shows the X-ray diffraction (XRD) of pristine $CH_3NH_3PbI_3$ perovskite ($MAPbI_3$), recovered perovskite from CH_3NH_2 gas treatment (MA-$MAPbI_3$) and bleached state film (Bleached $MAPbI_3$), that were deposited on FTO glass respectively. The pristine film shows the typical pattern of $CH_3NH_3PbI_3$ perovskite, with (110) peak located at 14.1°. After CH_3NH_2 gas treatment, the recovered perovskite phase shows a much stronger peak of (110) plane, as shown in Fig. 2d, indicating that the recovered film preferably orients along [110] direction. During the recovery of perovskite, the exfoliated layered perovskite intermediate preferentially restacks along the [110] direction, thereby resulting in high orientation of the recovered perovskite. The bleached film after longtime exposure clearly exhibits a predominant low angle peak at 7.1°. As shown in Fig. 2d, the intensity of peak is almost 30 times higher than (110) peak of pristine $CH_3NH_3PbI_3$ perovskite film. This suggests that the crystal structure of bleached film has a preferential orientation and a larger interplanar spacing. In comparison with the main peak of 14.1° for the pristine perovskite, the d-spacing increases from 6.25 Å to 12.41 Å with the intercalation of CH_3NH_2. The dimension of CH_3NH_2 molecule is ~1.43 Å (N-C distance), which implies that there are approximately 4 layers of CH_3NH_2 aligned between (110) planes, as demonstrated in Fig. 2b.

Fig. 2e shows the UV–vis absorption spectra of the three different films. Both pristine and recovered $CH_3NH_3PbI_3$ perovskite exhibit absorption edge at ~790 nm, corresponding to a band gap of 1.57 eV, which is consistent with the typical band gap of $CH_3NH_3PbI_3$ [30,31].

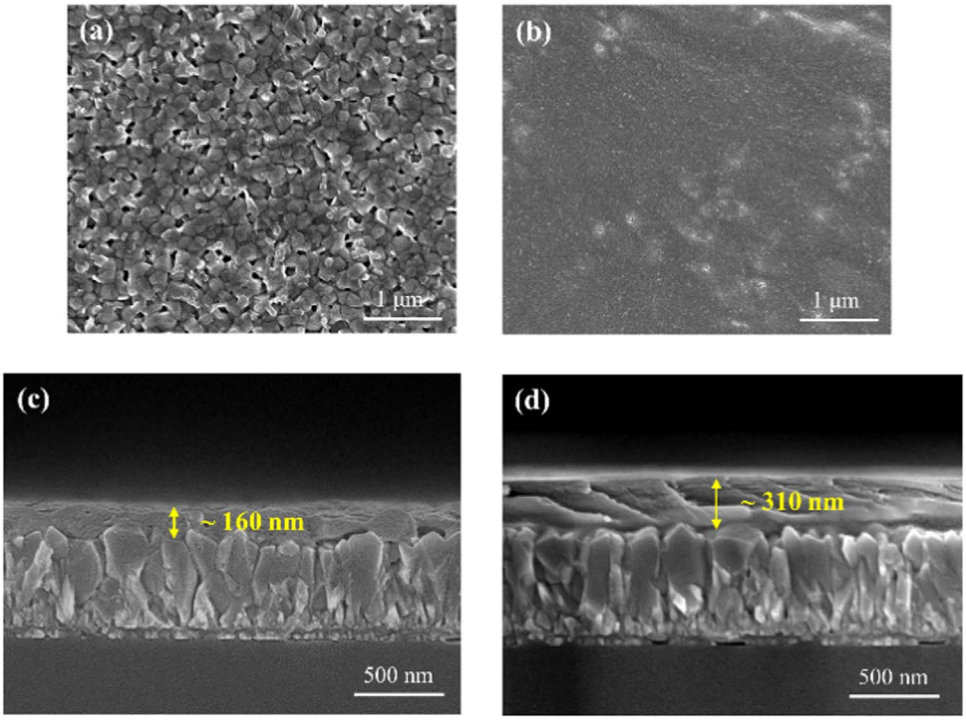

Fig. 3. Top surface SEM of (a) pristine $CH_3NH_3PbI_3$ perovskite and (b) bleached perovskite film. Cross-sectional SEM of (c) pristine $CH_3NH_3PbI_3$ perovskite and (d) bleached perovskite film.

However, for the bleached film, the main absorption feature is located at ~375 nm, which is assigned to the excitation from MX_6 octahedra [32]. Due to the incomplete conversion from 3D to 2D perovskite, there is a small amount of $CH_3NH_3PbI_3$ perovskite presenting in the film, as shown in the amplified spectrum of the bleached film (Fig. S2). The band gap of perovskite can be tuned through modulation of structural configuration. The transformation from 3D perovskite to 2D layered perovskite introduces Pb-I-Pb distortion, and the enlarged interplanar spacing of 2D perovskite weakens the orbital overlap between the two layers [16,33,34]. Both in-plane and out-of-plane configurational change of 2D perovskite lead to increase in band gap. The change in the band gap of 2D perovskite explains the dissimilar optical property between pristine $CH_3NH_3PbI_3$ perovskite film and bleached state film.

Fig. 3 shows the scanning electron microscopy (SEM) images of pristine $CH_3NH_3PbI_3$ film (a, c) and the bleached state film synthesized through longtime CH_3NH_2 gas exposure (b, d). The pristine $CH_3NH_3PbI_3$ film was synthesized by one-step anti-solvent treatment. It is noted that there are small pinholes distributed in the film (Fig. 3a), and the thickness of the film is ~160 nm (Fig. 3c). With exposure to CH_3NH_2 gas, the 3D perovskite structure was transformed into a 2D layered structure with the intercalation of CH_3NH_2 between (110) planes. From the SEM images of layered perovskite (Fig. 3b, d), it can be seen that films have very smooth and homogeneous surface. It can also be observed that a well-packed, highly oriented growth occurred and the thickness of the layered perovskite was increased to ~310 nm. The CH_3NH_2 intercalation expands the interplanar distance between the (110) planes, resulting in the increase of film thickness. Notably, the thickness of the layered film is approximately double of that pristine film, which is consistent with the increase in interplanar spacing calculated from XRD.

Through systematic investigation of the interaction between CH_3NH_2 and $CH_3NH_3PbI_3$ perovskite film, we revealed that CH_3NH_2 can slice 3D perovskite into 2D layered perovskites. We were able to demonstrate the slicing process on $CH_3NH_3PbI_3$ crystals with complete repeatability. With CH_3NH_2 exposure, the black perovskite crystals turn into a clear yellow liquid mixed with square bleached sheets, as shown in Fig. 4a. As discussed above, the induced CH_3NH_2 slices the 3D perovskite into colloidal sheets, resulting in a transition from 3D solid perovskite to a liquid phase. Motivated by the liquid state of $CH_3NH_3PbI_3$ perovskite, we directly utilized this liquid to prepare perovskite film. By using this type of liquid perovskite, a dark black film was achieved through spin coating. The liquid perovskite consists of dissociated layered MX_6 sheets with the intercalated CH_3NH_2. Upon deposition, owing to the high vapor pressure of CH_3NH_2, the excess CH_3NH_2 releases from the liquid perovskite, resulting in recrystallization of perovskite film. The XRD of the resultant film is shown in Fig. 4b. The film exhibits the tetragonal $CH_3NH_3PbI_3$ perovskite phase, with the main peak from (110) plane. In addition, the peak of PbI_2 phase was also observed in the pattern. Upon annealing the film at 100 °C for 10 min, the peak from (002) series plane disappeared (Fig. S3), indicating that further rearrangement occurs during the annealing process. Fig. 4d shows the SEM image of the film synthesized from liquid perovskite. The perovskite film shows a dendritic structure, which is probably due to fast crystallization. Fig. S4 shows the cross-sectional SEM of the film prepared from liquid perovskite exhibiting thickness of ~2.0 μm. To prepare perovskite solar cell, film thickness with micrometers are too large for optimum light absorption. Therefore, an appropriate solvent was employed to dilute the liquid perovskite to decrease the thickness of perovskite film. For this purpose, we adopted a sustainable solvent to replace the potentially toxic DMF as the solvent medium.

The aprotic and polar solvent is generally used to dissolve the perovskite precursor salts and among various possibilities, ACN has high polarity and is recommended in industrial production to enable the sustainable process [35]. Thus, the sustainable solvent, ACN, was used as the medium to prepare thinner perovskite films [36]. As shown in Fig. 4a, the $CH_3NH_3PbI_3$ crystals have very limited solubility in ACN. However, layered liquid perovskite was completely soluble in ACN. A clear, yellow solution was formed with the addition of ACN in the liquid perovskite. The ACN does not decompose the layered perovskites, and the exfoliated PbI_6 sheets uniformly disperse in ACN. We experimented with other greener solvent alternatives, water, ethanol, and isopropanol; however, these solvents led to either decomposition or insolubility with the liquid perovskite. Fig. 4b shows the XRD of perovskite films prepared from liquid perovskite, and perovskite ACN solution with and without the annealing process. As discussed earlier, the film prepared by liquid perovskite showed the pattern of perovskite and PbI_2. In contrast, film fabricated from the

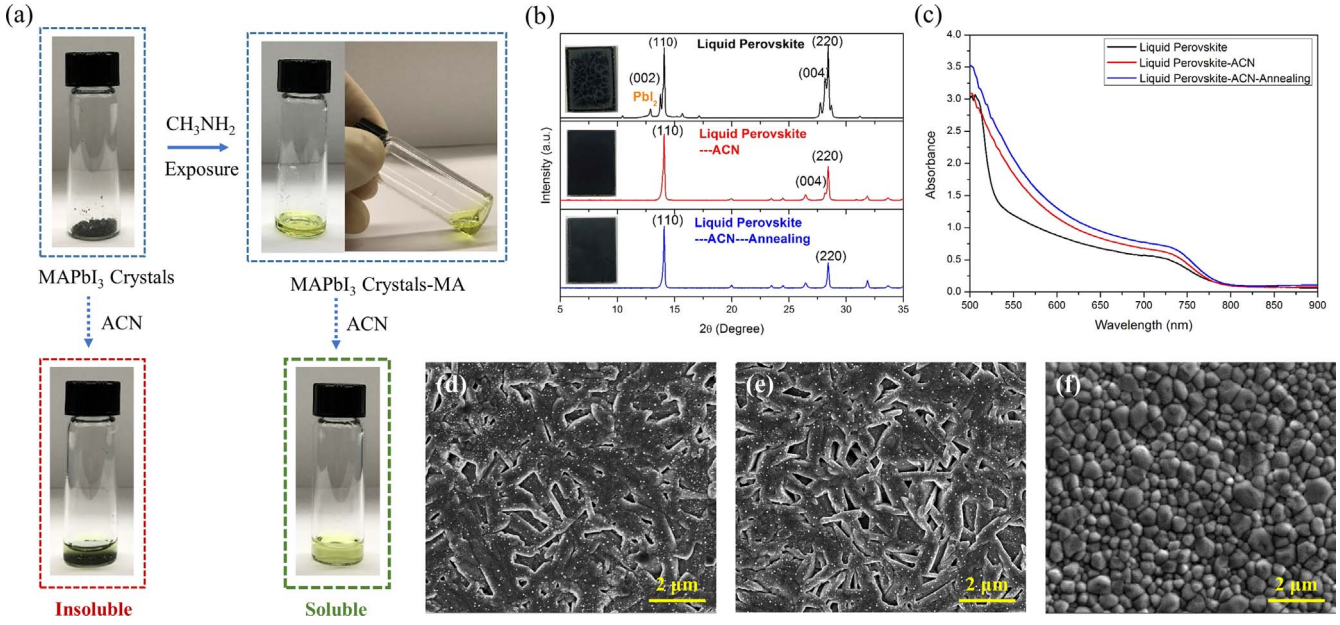

Fig. 4. (a) Pictorial illustration of the evolution of $CH_3NH_3PbI_3$ crystals under overnight CH_3NH_2 gas exposure. The resultant liquid perovskite was then dissolved in ACN. (b) XRD patterns and (c) UV–vis spectra of perovskite films fabricated by liquid perovskite, and liquid perovskite ACN solution with and without annealing process. Top surface SEM of perovskite films fabricated by liquid perovskite (d), perovskite ACN solution (e) without and (f) with annealing process.

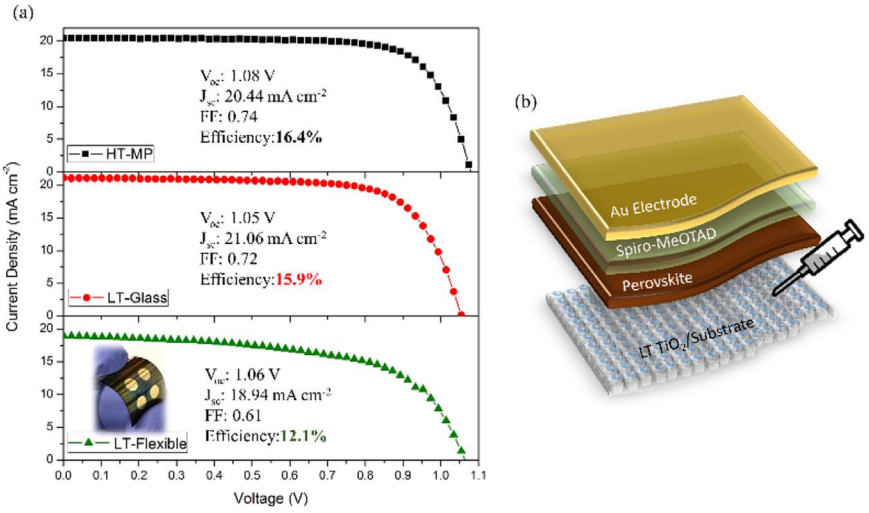

Fig. 5. (a) J-V characteristics of high-temperature mesoporous PSC, low-temperature glass based PSC and polymer based flexible PSC. (b) Schematics of low-temperature PSC structure and fabrication.

perovskite ACN solution showed pure tetragonal $CH_3NH_3PbI_3$ pattern without the presence of PbI_2. As seen in XRD, at 2θ=28.2°, the peak was split into two peaks, corresponding to (220) and (004) planes. Upon annealing at 100 °C, the XRD pattern almost remains identical, but (004) peak disappears. Fig. 4c shows the UV–vis absorption spectra of the synthesized films. The film fabricated from liquid perovskite shows both absorption edge of $CH_3NH_3PbI_3$ and of PbI_2, which are located at ~790 nm and ~530 nm respectively. For the film prepared from perovskite ACN solution, both of them exhibit the typical absorption features of $CH_3NH_3PbI_3$ perovskite. Fig. 4d, e, and f compare the surface morphology of the films prepared by liquid perovskite, and perovskite ACN solution without and with annealing. As discussed earlier, the film from liquid perovskite shows dendritic morphology. The perovskite film prepared from ACN solution still exhibits dendritic structure but with holes distributed in the film, which may be attributed to the dilution from the addition of ACN. However, upon annealing, the morphology transformed from the columnar dendrite perovskite to hexagonal perovskite grains. During the annealing process, driven by the surface energy reduction of the crystals, dendrite crystals convert to hexagonal crystal [37]. In addition, the perovskite film shows homogeneous surface, and the thickness of the perovskite film is ~520 nm (Fig. S5), which is suitable for use as the light absorber for PSCs. The annealing process not only provides thermal energy to facilitate the structural evolution but also promotes the release of ACN and CH_3NH_2 from the layered PbI_6 sheets. We also used vacuum process to treat the film fabricated by the perovskite ACN solution. Fig. S6 shows the XRD and top surface morphology of the film following vacuum process. The XRD of the film after vacuum treatment is very similar with the annealed one, with a predominance of (110) series planes. In addition, the film also shows a surface with hexagonal crystals, but the film is rougher than the annealed one. The results suggest that similar to annealing, the vacuum process also assists the release of ACN and CH_3NH_2 and thus favors the formation of hexagonal perovskites.

To study the photovoltaic performance of PSCs fabricated by the slicing of 3D crystals and restacking 2D layers, we first prepared PSCs with TiO_2 mesoporous architecture, which was annealed at 500 °C. The J-V characteristics of PSCs prepared from the perovskite ACN solution (concentration: 1.0 M) without treatment, and with annealing and vacuum process are shown in Fig. S7. The PSC without any further treatment exhibited conversion efficiency of 6.13%. This low efficiency was probably due to the dendrite and porous perovskite structure. Following annealing, the efficiency of PSC was boosted to 16.4%, with V_{oc} of 1.08 V, J_{sc} of 20.44 mA cm^{-2} and FF of 0.74. However, for the vacuum processed sample, the PSC shows a lower efficiency of 11.5%. The results indicate that in comparison with vacuum process, the annealing could more effectively favor the release of CH_3NH_2 and result in the uniform hexagonal perovskite film, which leads to improvement in conversion efficiency. The thickness of perovskite layer has a crucial influence on the performance of PSCs. We modified the thickness of perovskite by controlling the concentration of perovskite ACN solution. When the concentration was increased to 1.3 M, owing to the high internal stresses, cracks began to form within the perovskite layer. Thus, we synthesized the perovskite layer with concentrations of 1.0 M, 0.8 M, and 0.67 M. The perovskite layers show the thickness of ~520 nm for 1.0 M concentration, ~410 nm for 0.8 M and ~330 nm for 0.67 M, as shown in Fig. S8. The J-V characteristics are presented in Fig. S9. Compared with 1.0 M concentration, the PSCs with concentrations of 0. 8 M and 0.67 M show lower conversion efficiency of 14.9% and 12.3% respectively. Thus in the following experiments, the perovskite layers were synthesized by annealing process using the concentration of 1.0 M.

The facile one-step fabrication of PSC with a sustainable solvent motivated us to prepare low temperature processed cells. The low-temperature cell eliminates the high-temperature annealing process, which could improve the manufacturing productivity and enable fabrication on the flexible polymer substrate. The schematic structure of the low-temperature PSC is shown in Fig. 5b, where the low temperature synthesized TiO_2 compact layer is based on solution process method [21]. For the low-temperature PSC, the conversion efficiency was 15.9%, with V_{oc} of 1.05 V, J_{sc} of 21.06 mA cm^{-2} and FF of 0.72 (Fig. 5a), showing close performance with that of the high-temperature mesoporous PSC. We further applied the low temperature processed TiO_2 compact layer on flexible polymer substrate (ITO/PEN). As shown in the J-V curve of low-temperature flexible PSC, the flexible PSC shows V_{oc} of 1.06 V, J_{sc} of 18.94 mA cm^{-2}, FF of 0.61, yielding a conversion efficiency of 12.1%. The main difference between low-temperature glass PSC and flexible PSC is the fill factor, which is mainly due to the high ohmic resistance of the polymer substrate. Availability of flexible substrates with higher conductivity will result in enhanced photovoltaic performance of flexible cell that can be comparable with glass PSC.

The inherent moisture stability of perovskite layer remains the main challenge for PSCs commercialization. In order to study the moisture stability of perovskite synthesized by slicing-restacking process, we compared the stability of perovskite films fabricated by the conventional method (anti-solvent) and slicing-restacking method. Fig. S10 shows the XRD of these two perovskite films exposed to 60%

humid air for 7 days. The $CH_3NH_3PbI_3$ perovskite synthesized by conventional method gradually decomposes to PbI_2 during the 7 days of testing. However, $CH_3NH_3PbI_3$ perovskite fabricated by slicing-restacking process shows no change, and no PbI_2 was detected in XRD spectra. The improvement in moisture stability for the perovskite synthesized by slicing-restacking process is attributed to the highly oriented and well-stacked perovskite, which leads to the reduced grain boundary defects, thus preventing the moisture penetration through grain boundary.

4. Conclusion

We have developed a slicing and restacking process for facile fabrication of $CH_3NH_3PbI_3$ perovskite film. This fabrication process utilizes a sustainable solvent alternative and enables simple one-step deposition, which is completely compatible with the large-scale printable production process. The induced CH_3NH_2 was shown to slice the 3D $CH_3NH_3PbI_3$ crystals into 2D layered perovskite intermediates along [110] direction. With the increase in the CH_3NH_2 exposure time, the CH_3NH_2 intercalated between the MX_6 layers forming a well-stacked 2D perovskite sheet. Surprisingly, the layered intermediate phase showed high solubility in a sustainable solvent ACN. This synthesis method could replace the commonly used, potentially toxic DMF as the solvent, enabling a sustainable manufacturing. By using this perovskite ACN solution, high-quality $CH_3NH_3PbI_3$ perovskite film can be readily prepared via simple one-step synthesis. Based on this approach, we prepared cells using high-temperature annealing, low-temperature TiO_2 paste and flexible substrate which exhibited conversion efficiencies of 16.4%, 15.9%, and 12.1%, respectively. This new approach not only reveals an approach for transformation from 3D to 2D layered perovskite but also provides a sustainable and productive fabrication method for PSCs, paving the way for scaling perovskite solar cell manufacturing.

Acknowledgements

The authors acknowledge the financial support from the Institute of Critical Technology and Applied Science (ICTAS). Authors S.P. would like to acknowledge the financial support from Office of Naval Research (I. Perez). Y.Y. was supported through the AMRDEC participation in NSF I/UCRC: Center for Energy Harvesting Materials and Systems (CEHMS).

Appendix A. Supporting information

Supplementary data associated with this article can be found in the online version at doi:10.1016/j.nanoen.2017.04.034.

References

[1] H.J. Snaith, Perovskites: the emergence of a new era for low-cost, high-efficiency solar cells, J. Phys. Chem. Lett. 4 (2013) 3623–3630.
[2] S.T. Williams, A. Rajagopal, C.C. Chueh, A.K.Y. Jen, Current challenges and prospective research for upscaling hybrid perovskite photovoltaics, J. Phys. Chem. Lett. 7 (2016) 811–819.
[3] NREL soalr cell efficiency chart.
[4] N. Sakai, S. Pathak, H.-W. Chen, A.A. Haghighirad, S.D. Stranks, T. Miyasaka, H.J. Snaith, The mechanism of toluene-assisted crystallization of organic–inorganic perovskites for highly efficient solar cells, J. Mater. Chem. A 4 (2016) 4464–4471.
[5] N.J. Jeon, J.H. Noh, Y.C. Kim, W.S. Yang, S. Ryu, S. Il Seok, Solvent engineering for high-performance inorganic–organic hybrid perovskite solar cells, Nat. Mater. 13 (2014) 897–903.
[6] L. Zuo, Z. Gu, T. Ye, W. Fu, G. Wu, H. Li, H. Chen, Enhanced photovoltaic performance of $CH_3NH_3PbI_3$ perovskite solar cells through interfacial engineering using self-assembling monolayer, J. Am. Chem. Soc. 137 (2015) 2674–2679.
[7] C. Bi, Q. Wang, Y. Shao, Y. Yuan, Z. Xiao, J. Huang, Non-wetting surface-driven high-aspect-ratio crystalline grain growth for efficient hybrid perovskite solar cells, Nat. Commun. 6 (2015) 7747.
[8] C. Wehrenfennig, G.E. Eperon, M.B. Johnston, H.J. Snaith, L.M. Herz, High charge carrier mobilities and lifetimes in organolead trihalide perovskites, Adv. Mater. 26 (2014) 1584–1589.
[9] M. Yang, Y. Zhou, Y. Zeng, C.-S. Jiang, N.P. Padture, K. Zhu, Square-centimeter solution-processed planar $CH_3NH_3PbI_3$ perovskite solar cells with efficiency exceeding 15%, Adv. Mater. 27 (2015) 6363–6370.
[10] C. Liu, K. Wang, C. Yi, X. Shi, A.W. Smith, X. Gong, A.J. Heeger, Efficient perovskite hybrid photovoltaics via alcohol-vapor annealing treatment, Adv. Funct. Mater. 26 (2016) 101–110.
[11] Z. Xiao, Q. Dong, C. Bi, Y. Shao, Y. Yuan, J. Huang, Solvent annealing of perovskite-induced crystal growth for photovoltaic-device efficiency enhancement, Adv. Mater. 26 (2014) 6503–6509.
[12] J. Liu, C. Gao, X. He, Q. Ye, L. Ouyang, D. Zhuang, C. Liao, J. Mei, W. Lau, Improved crystallization of perovskite films by optimized solvent annealing for high efficiency solar cell, ACS Appl. Mater. Interfaces 7 (2015) 24008–24015.
[13] M. Liu, M.B. Johnston, H.J. Snaith, Efficient planar heterojunction perovskite solar cells by vapour deposition, Nature 501 (2013) 395–398.
[14] D. Shi, V. Adinolfi, R. Comin, M. Yuan, E. Alarousu, A. Buin, Y. Chen, S. Hoogland, A. Rothenberger, K. Katsiev, Y. Losovyj, X. Zhang, P.A. Dowben, O.F. Mohammed, E.H. Sargent, O.M. Bakr, Low trap-state density and long carrier diffusion in organolead trihalide perovskite single crystals, Science 347 (2015) 519–522.
[15] B. Saparov, D.B. Mitzi, Organic-inorganic perovskites: structural versatility for functional materials design, Chem. Rev. 116 (2016) 4558–4596.
[16] M.E. Kamminga, H.-H. Fang, M.R. Filip, F. Giustino, J. Baas, G.R. Blake, M.A. Loi, T.T.M. Palstra, Confinement effects in low-dimensional lead iodide perovskite hybrids, Chem. Mater. 28 (2016) 4554–4562.
[17] H. Tsai, W. Nie, J.-C. Blancon, C.C. Stoumpos, R. Asadpour, B. Harutyunyan, A.J. Neukirch, R. Verduzco, J.J. Crochet, S. Tretiak, L. Pedesseau, J. Even, M.A. Alam, G. Gupta, J. Lou, P.M. Ajayan, M.J. Bedzyk, M.G. Kanatzidis, A.D. Mohite, High-efficiency two-dimensional Ruddlesden–Popper perovskite solar cells, Nature 536 (2016) 312–316.
[18] Z. Zhou, Z. Wang, Y. Zhou, S. Pang, D. Wang, H. Xu, Z. Liu, N.P. Padture, G. Cui, Methylamine-gas-induced defect-healing behavior of $CH_3NH_3PbI_3$ thin films for perovskite solar cells, Angew. Chem. Int. Ed. 54 (2015) 9705–9709.
[19] F.P. Byrne, S. Jin, G. Paggiola, T.H.M. Petchey, J.H. Clark, T.J. Farmer, A.J. Hunt, C. Robert McElroy, J. Sherwood, Tools and techniques for solvent selection: green solvent selection guides, Sustain. Chem. Process. 4 (2016) 7.
[20] V. Kozell, M. McLaughlin, G. Strappaveccia, S. Santoro, L.A. Bivona, C. Aprile, M. Gruttadauria, L. Vaccaro, Sustainable approach to waste-minimized Sonogashira cross-coupling reaction based on recoverable/reusable heterogeneous catalytic/base system and acetonitrile azeotrope, ACS Sustain. Chem. Eng. 4 (2016) 7209–7216.
[21] C. Wu, X. Zheng, Q. Yang, Y. Yan, M. Sanghadasa, S. Priya, Crystallization of $HC(NH_2)_2$ PbI_3 black polymorph by solvent intercalation for low temperature solution processing of perovskite solar cells, J. Phys. Chem. C 120 (2016) 26710–26719.
[22] D.B. Mitzi, Synthesis, structure, and properties of organic-inorganic perovskites and related materials, Prog. Inorg. Chem. (2007) 1–121.
[23] D.B. Mitzi, Templating and structural engineering in organic-inorganic perovskites, J. Chem. Soc. Dalt.on Trans. (2001) 1–12.
[24] D.H. Cao, C.C. Stoumpos, O.K. Farha, J.T. Hupp, M.G. Kanatzidis, 2D homologous perovskites as light-absorbing materials for solar cell applications, J. Am. Chem. Soc. 137 (2015) 7843–7850.
[25] I.C. Smith, E.T. Hoke, D. Solis-Ibarra, M.D. McGehee, H.I. Karunadasa, A. Layered, Hybrid perovskite solar-cell absorber with enhanced moisture stability, Angew. Chem. Int. Ed. 53 (2014) 11232–11235.
[26] C.C. Stoumpos, D.H. Cao, D.J. Clark, J. Young, J.M. Rondinelli, J.I. Jang, J.T. Hupp, M.G. Kanatzidis, Ruddlesden-Popper hybrid lead iodide perovskite 2D homologous semiconductors, Chem. Mater. 28 (2016) 2852–2867.
[27] D.J. Bacon, V. Vitek, Atomic-scale modeling of dislocations and related properties in the hexagonal-close-packed metals, Metall. Mater. Trans. A 33 (2002) 721–733.
[28] M.H. Yoo, Slip, twinning, and fracture in hexagonal close-packed metals, Metall. Trans. A 12 (1981) 409–418.
[29] D.B. Mitzi, D.R. Medeiros, P.R.L. Malenfant, Intercalated organic-inorganic perovskites stabilized by fluoroaryl-aryl interactions, Inorg. Chem. 41 (2002) 2134–2145.
[30] G.E. Eperon, S.D. Stranks, C. Menelaou, M.B. Johnston, L.M. Herz, H.J. Snaith, Formamidinium lead trihalide: a broadly tunable perovskite for efficient planar heterojunction solar cells, Energy Environ. Sci. 7 (2014) 982–988.
[31] J.H. Noh, S.H. Im, J.H. Heo, T.N. Mandal, S. Il Seok, Chemical management for colorful, efficient, and stable inorganic–organic hybrid nanostructured solar cells, Nano Lett. 13 (2013) 1764–1769.
[32] Y. Tabuchi, K. Asai, M. Rikukawa, K. Sanui, K. Ishigure, Preparation and characterization of natural lower dimensional layered perovskite-type compounds, J. Phys. Chem. Solids 61 (2000) 837–845.
[33] C.C. Stoumpos, L. Mao, C.D. Malliakas, M.G. Kanatzidis, Structure–band gap relationships in hexagonal polytypes and low-dimensional structures of hybrid tin iodide perovskites, Inorg. Chem. 56 (2017) 56–73.
[34] J. Androulakis, S.C. Peter, H. Li, C.D. Malliakas, J.A. Peters, Z. Liu, B.W. Wessels, J.-H. Song, H. Jin, A.J. Freeman, M.G. Kanatzidis, Dimensional reduction: a design tool for new radiation detection materials, Adv. Mater. 23 (2011) 4163–4167.
[35] D. Prat, O. Pardigon, H.-W. Flemming, S. Letestu, V. Ducandas, P. Isnard, E. Guntrum, T. Senac, S. Ruisseau, P. Cruciani, P. Hosek, Sanofi's solvent selection guide: a step toward more sustainable processes, Org. Process Res. Dev. 17 (2013) 1517–1525.
[36] N.K. Noel, S.N. Habisreutinger, B. Wenger, M.T. Klug, M.T. Hörantner, M.B. Johnston, R.J. Nicholas, D.T. Moore, H.J. Snaith, A low viscosity, low boiling

point, clean solvent system for the rapid crystallisation of highly specular perovskite films, Energy Environ. Sci. 10 (2017) 145–152.
[37] D. Bi, C. Yi, J. Luo, J.-D. Décoppet, F. Zhang, S.M. Zakeeruddin, X. Li, A. Hagfeldt, M. Grätzel, Polymer-templated nucleation and crystal growth of perovskite films for solar cells with efficiency greater than 21%, Nat. Energy 1 (2016) 16142.

Dr. Congcong Wu is currently a Research Associate in the Center for Energy Harvesting Materials and Systems (CEHMS) at Virginia Tech, United States. He received his B.S. degree and Ph.D. degree in Material Science from Huazhong University of Science and Technology in 2007 and 2014, respectively. His research interests include energy harvesting, printed and flexible electronics, nanostructure materials, and new types of solar cells. During the period of Ph.D. study, he conducted research on one-dimensional nanomaterials and high-performance polymer electrolytes for dye-sensitized solar cell. Currently, he is leading research towards scaling-up of stable perovskite solar cells on the flexible substrate.

Haijin Li is currently a Ph.D. candidate in Center for Fuel Cell Innovation, School of Materials Science and Engineering, Huazhong University of Science & Technology. He is now working at Center for Energy Harvesting Materials and System (CEHMS), Virginia Tech as a visiting researcher. His research focuses on dye-sensitized solar cells, quantum dot sensitized solar cells, perovskite solar cells and inorganic nanomaterials for photovoltaics.

Dr. Yongke Yan is a Research Assistant Professor in the ICTAS and the Center for Energy Harvesting Materials and Systems (CEHMS) at Virginia Tech, USA. He received his B.E. degree in Metal Material Engineering from Central South University, China, in 2003, and Ph.D. degree in Materials Science and Engineering from Tsinghua University, China, in 2008. Before joined CEHMS in Virginia Tech in 2010, he conducted his postdoc research in National Institute for Materials Science (NIMS), Japan. His research interests include dielectric, ferroelectric, piezoelectric, magnetic, magnetoelectric materials & devices; solid oxide fuel cells.

Dr. Bo Chi is a professor at Center for Fuel Cell Innovation, School of Materials Science and Technology at Huazhong University of Science and Technology, China. He received his BS and master degree in Materials Science from China University of Geosciences (Wuhan) in 1998 and 2001, respectively, and his PhD degree in Materials Science from Tsinghua University in 2005. His current research interests are in the areas of solid oxide fuel cell (SOFC), solid oxide electrolytic cell (SOEC), and solar cell.

Dr. Jian Pu is a professor at Center for Fuel Cell Innovation, School of Materials Science and Technology at Huazhong University of Science and Technology, China. He received his ME Sc and PhD degree in Materials Science from Huazhong University of Science and Technology in 2001 and 2004, respectively. His current research interests are in the areas of solid oxide fuel cell (SOFC), solar cell, and oxygen sensors.

Dr. Jian Li is a professor at Center for Fuel Cell Innovation, School of Materials Science and Technology at Huazhong University of Science and Technology, China. He received his BS and ME Sc in Materials Science from Shanghai Jiao Tong University in 1982 and 1985, respectively, and his PhD degrees in Metallurgy from Iron and Steel Research Institute of China in 1988 and in Ceramics from University of Illinois at Urbana-Champaign in 1995. His current research interests are in the areas of solid oxide fuel cell (SOFC), solar cell, and high-strength steel.

Dr. Mohan Sanghadasa is a senior research scientist at US Army AMRDEC. He currently leads research programs on the development of nanotechnology enhanced sensors and energy storage systems. His previous research activities at AMRDEC was on the development of polymer based modulators for IFOGs in inertial measurement units. He joined AMRDEC following 12 years on the faculty of University of Alabama in Huntsville (UAH). His research activities at UAH was primarily in the area of nonlinear optics. During his academic career, Dr. Sanghadasa has also conducted research on optical limiting, optical switching, and optical pattern recognition.

Dr. Shashank Priya is currently Robert E Hord Jr. Professor in department of mechanical engineering. He is also serving as associate director of research and scholarship at Institute for Critical Technology and Applied Science. Dr. Priya has made strong impact in the field of energy harvesting, multifunctional materials, and bio-inspired robotics. He has published over 325 peer-reviewed publications covering these topics. Additionally, he has published 60 conference proceedings, four US patents and five edited books. He is founder and chair of Annual Energy Harvesting Workshop series (www.ehworkshop.-com). Dr. Priya is currently serving as founding president of energy harvesting society (www.energyharvestingsociety.org), and member of the Honorary Chair Committee, for the International Workshop on Piezoelectric Materials and Applications (IWPMA).